Monatsh Chem (2011) 142:585–592
DOI 10.1007/s00706-011-0502-x

ORIGINAL PAPER

DFT and MM description of the structure and magnetic properties of manganese complexes with X-phenylcyanamido bridging ligand

Marko Perić · Svetozar Niketić · Matija Zlatar · Maja Gruden-Pavlović · Sonja Grubišić

Received: 18 February 2011 / Accepted: 30 March 2011 / Published online: 28 April 2011

Abstract Magnetic properties of the complexes [Mn(3-Clpcyd)(H_2O)-(phen)$_2$]$^+$, [{Mn(3-Fpcyd)(MeOH)(phen)}$_2$(μ-3-Fpcyd)$_2$], [{Mn(3-Fpcyd)(EtOH)(phen)}$_2$(μ-3-Fpcyd)$_2$], [{Mn(3-Clpcyd)(MeOH)(phen)}$_2$(μ-3-Clpcyd)$_2$], and [{Mn(4-Clpcyd)(EtOH)(phen)}$_2$(μ-4-Clpcyd)$_2$] (where Xpcyd = halogeno-phenylcyanamido; phen = 1,10-phenanthroline) have been explored by means of density functional theory (DFT). Exchange coupling constants were calculated from the energy differences between the high-spin and broken-symmetry states. Very good agreement between theoretical and experimental data was achieved. The g-tensor calculations were performed employing the coupled perturbed Kohn–Sham equations. Molecular mechanics calculations have been performed to elucidate structural features in the five complexes. Finally, the reliability of the molecular mechanics results was confirmed by comparing the magnetic couplings calculated on optimized structures with experimental data.

Keywords Quantum chemical calculations · Force-field calculations · Transition-metal compounds · Magnetic couplings · Zero-field splitting

Electronic supplementary material The online version of this article (doi:10.1007/s00706-011-0502-x) contains supplementary material, which is available to authorized users.

M. Perić · S. Niketić · M. Zlatar · S. Grubišić (✉)
Center for Chemistry, Institute of Chemistry, Technology and Metallurgy, University of Belgrade, Njegoševa 12, P.O. Box 815, 11001 Belgrade, Serbia
e-mail: grubisic@chem.bg.ac.rs

M. Gruden-Pavlović
Faculty of Chemistry, University of Belgrade, Studentski trg 16, P.O. Box 158, 11001 Belgrade, Serbia

Introduction

Understanding the origin of the spectroscopic and magnetic properties of transition-metal complexes has been a subject of interest to many authors [1–9]. Computational quantum chemistry has made enormous progress in the last 30 years. Nevertheless, understanding of the spectroscopic and magnetic properties of transition-metal compounds is still far from perfect. Since magnetic interactions arise from the electrostatic interaction between electrons in the molecules, which causes electronic states with different spin multiplicity to be close in energy, their description requires the use of computational approaches that can handle electron correlation at the highest level of accuracy. Density functional theory (DFT) has been widely applied to compute the magnetic properties of binuclear transition-metal complexes because of the low central processing unit (CPU) cost/accuracy ratio achieved by this formalism, allowing one to handle chemically complex systems.

Although the theoretical framework used nowadays for calculations of magnetic properties is well described in literature [9–17], for the sake of clarity, here we briefly recall the main points. The most general spin Hamiltonian derived by Pryce and Abragam and relevant to the work described in this paper is presented in Eq. 1 [11, 12].

$$\hat{H} = -2J\,\hat{S}_1\,\hat{S}_2 + \sum_{i=1}\mu_B\,\vec{B}\,g_i\hat{S}_i + \sum_{i=1}\hat{S}_i\,D_i\,\hat{S}_i + \ldots \qquad (1)$$

The first term in Eq. 1 arises due to the exchange interactions. In the investigated systems, the exchange coupling constant between the two metal centers, J, is computed using the broken-symmetry approach developed by Noodleman et al. [13–16].

The exchange coupling constant, J, can be estimated according to the Yamaguchi approach using Eq. 2 [17, 18].

$$J = \frac{(E_{HS} - E_{BS})}{\langle S^2\rangle_{HS} - \langle S^2\rangle_{BS}}, \quad (2)$$

where E_{HS} is the energy of the high spin, E_{BS} is the energy of the broken symmetry, and $\langle S^2\rangle_{HS}$ and $\langle S^2\rangle_{BS}$ are the expectation values of the high-spin and broken-symmetry $\hat{S}^2$ operators. If the metal centers are ferromagnetically coupled, J is positive because the highest spin state lies lower in energy. On the other hand, antiferromagnetic coupling yields a negative value of J and the lowest spin state is the ground state.

The interaction between a magnetic field and the electron spin is described by the second term in Eq. 1, where μ_B is Bohr's magneton, $\vec{B}$ is the magnetic flux density, S is the fictitious electron spin, and g is a gyromagnetic tensor or g-tensor. The gyromagnetic tensor can be separated into the different contributions as follows: $g = g_e + \Delta g^{RMC} + \Delta g^{GC} + \Delta g^{OZ/SOC}$, where g_e is the free electron value ($g_e = 2.0023$). Computation of the relativistic mass correction (RMC) and gauge correction (GC) is quite straightforward, because they are first-order contributions [19]. The main contribution to the g anisotropy and the deviation from the free electron value, g_e, comes from the last term, corresponding to orbital Zeeman/spin–orbit couplings (OZ/SOC) corrections. The aim of the theoretical treatment is to predict the values of the elements of the g-tensor.

For the binuclear complexes, molecular g-tensors of the high-spin and the broken-symmetry states were calculated by employing the coupled perturbed Kohn–Sham equations with an effective one-electron approximation of the spin–orbit contribution operator [20–23]. The g-matrices of the HS and BS states were used for the calculation of the g-tensor site matrices g_1 (Eq. 3) and g_2 (Eq. 4) as

$$g_1 = \frac{1}{2S_1}\left(g_{HS}M_S^{HS} + g_{BS}M_S^{BS}\right), \quad (3)$$

$$g_2 = \frac{1}{2S_2}\left(g_{HS}M_S^{HS} - g_{BS}M_S^{BS}\right). \quad (4)$$

These matrices were employed for the computation of the g-tensor of the antiferromagnetic (AF) state by multiplication with the respective spin projection coefficients c_i (Eq. 5) as

$$g = c_1 g_1 + c_2 g_2 + \frac{c_1 c_2}{5J}(g_1 - g_2) \times [(3c_1 + 1)d_1 - (3c_2 + 1)d_2]. \quad (5)$$

For the present system, the spin projection coefficients are $c_1 = c_2 = 1/2$. The local tensors d_1 and d_2 express the zero-field splitting (ZFS) of metal ions.

In the spin Hamiltonian formalism (Eq. 1) the zero-field splitting tensor D describes the splitting of the magnetic sublevels of an orbitally nondegenerate state with total spin $S > ½$ in the absence of a magnetic field [9, 24, 25]. From the point of view of quantum chemistry, this term has two contributions that arise from the direct magnetic spin–spin (SS) dipole–dipole interaction (due to the first-order perturbation theory) and from the spin–orbit coupling (due to the second-order perturbation theory).

The SOC part of the ZFS has four excitation contributions: (1) excitation from α semi-occupied molecular orbital (SOMO) to α virtual molecular orbital (VMO), leading to the same spin state, (2) excitation from β doubly occupied molecular orbital (DOMO) to β SOMO, also leading to the same spin state as the ground state, (3) excitation from α SOMO to β SOMO, leading to states with $S' = S - 1$, and (4) excitation from β DOMO to α VMO, leading to states with $S' = S + 1$.

In the spin-unrestricted Kohn–Sham (UKS) formalism, the Pederson–Khanna (PK) equation for the same spin contributions is Eq. 6.

$$D_{\mu\nu} = -\sum_{\sigma\sigma'=\alpha\beta}\frac{(-1)^{\sigma+\sigma'}}{4S^2}\sum_{i\in\sigma}\sum_{a\in\sigma'}\frac{\left\langle\Psi_i^{\sigma}\middle|h_\mu^{SOC}\middle|\Psi_a^{\sigma'}\right\rangle\left\langle\Psi_a^{\sigma'}\middle|h_\nu^{SOC}\middle|\Psi_i^{\sigma}\right\rangle}{\varepsilon_{a\sigma'} - \varepsilon_{i\sigma}}. \quad (6)$$

Here S is the ground-state spin, $\sigma\sigma' = \alpha\beta$ are "spin-channels," ψ^σ are the occupied molecular orbitals (MOs) of spin σ with orbital energy $\varepsilon_{i\sigma}$, and $\psi_a^{\sigma'}$ are the unoccupied MOs of σ' with orbital energy $\varepsilon_{i\sigma'}$. The operators h_μ^{SOC} are the spatial parts of the effective one-electron SOC treatment. Although this approach is the most widely used, it generally underestimates D_{SOC}, especially in the case of transition-metal monomers. A recently derived linear response method based on a coupled perturbed (CP) SOC approach has been proposed [26, 27]. In this work, ZFS data obtained by these two approaches have been compared.

The magnetic behavior of transition-metal complexes containing more than one paramagnetic metal center bridged through multi-atomic ligands often differs from that assumed by the sum of the magnetic properties of each individual unit bearing unpaired electrons. It was found that the magnetic properties of binuclear species depend on the metal–metal distances, bond angles between bridging atoms, dihedral angles between planes including metal centers, bond distances, and coordination environments around the metals [10]. The continuing interest in characterization of polynuclear manganese complexes arises mainly from their relevance in molecular magnetism and in biological systems, since manganese is known to exist at the active centers of several redox enzymes.

The ability of the dicyanamido ($dicyd^{2-}$) type of bridging ligands to mediate metal–metal coupling suggests that also phenylcyanamide (pcyd) derivatives may have useful electronic and/or magnetic properties [28].

Phenylcyanamide ligands are interesting and practically unexplored ligands from the magnetic point of view. The first magnetic measurements on systems containing the Mn(II)–$(NCN)_2$–Mn(II) unit, where the cyanamido group (NCN) is coordinated in end-to-end mode, were reported by Escuer et al. [29, 30]. In those preliminary works, they demonstrated the ability of this kind of bridge to transmit moderate antiferromagnetic coupling. It has been proposed, on the basis of extended-Hückel MO calculations, that the $\mu_{1,3}$-NCN pcyd ligands have an intermediate place between azido and dicyanamido as superexchange mediators [29]. Following that work, with pcyd type of ligands five new Mn^{II}/Xpcyd compounds in combination with the blocking 1,10-phenanthroline ligand (phen) have been synthesized and characterized [31]. These compounds contain the unusual end-to-end R-cyanamide bridge and give supramolecular one-dimensional networks by means of H-bonds involving the N-amide atoms of the phenylcyanamide ligands.

We have performed density functional theory (DFT) calculations of the magnetic properties on X-ray and molecular mechanics (MM)-optimized structures of mono- and binuclear Mn(II) complexes **1**–**5** with X-phenylcyanamido bridging ligands (Fig. 1) to gain better insight into the origin of phenomena.

For the Mn(II) ion, the ZFS parameter is highly sensitive to the environment of the central metal ion, so very important structural information can be obtained.

Mononuclear units can be coupled in polynuclear complexes with a large negative magnetic anisotropy (single molecular magnets, SMM), so the evaluation of ZFS parameters is of great importance.

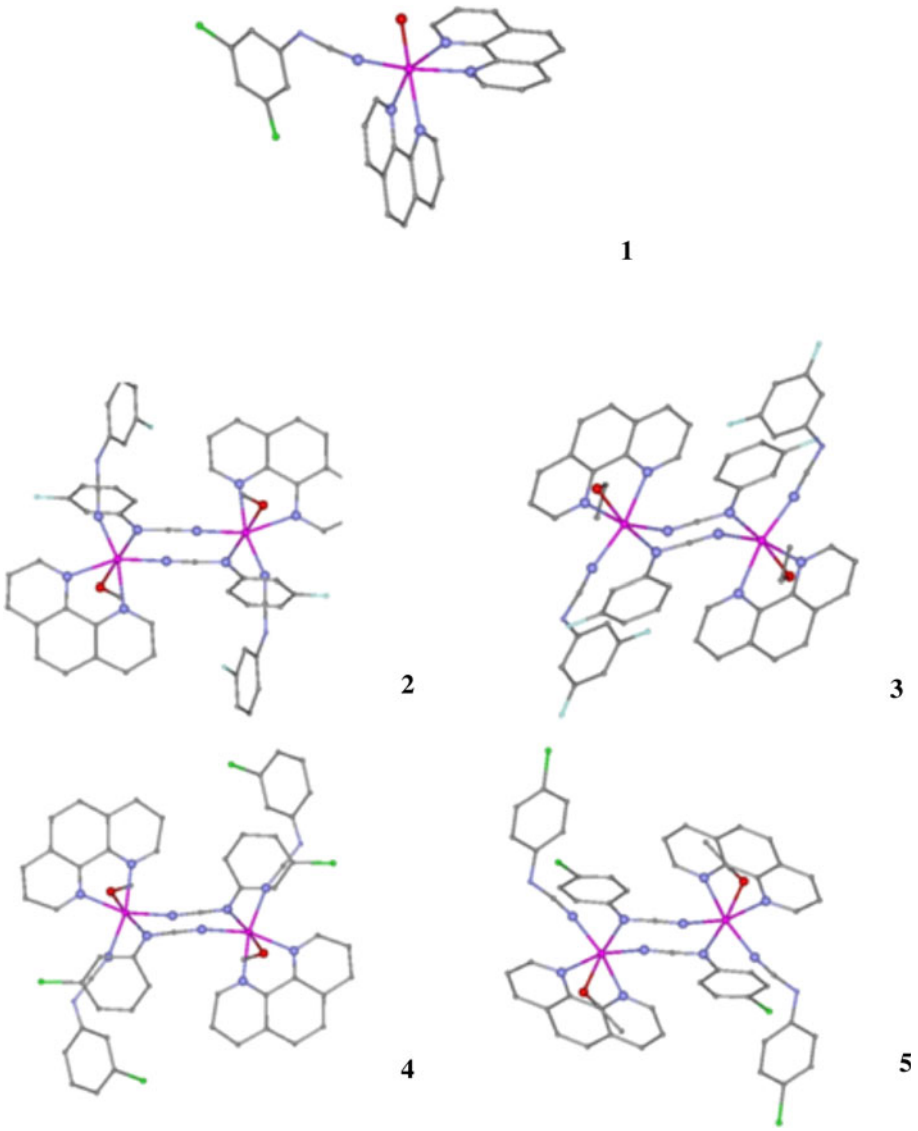

Fig. 1 Representation of the Mn(II) complexes **1**–**5** studied in this work: $[Mn(3\text{-}Clpcyd)(H_2O)\text{-}(phen)_2]^+$ (**1**), $[\{Mn(3\text{-}Fpcyd)(MeOH)(phen)\}_2(\mu\text{-}3\text{-}Fpcyd)_2]$ (**2**), $[\{Mn(3\text{-}Fpcyd)(EtOH)(phen)\}_2(\mu\text{-}3\text{-}Fpcyd)_2]$ (**3**), $[\{Mn(3\text{-}Clpcyd)(MeOH)(phen)\}_2(\mu\text{-}3\text{-}Clpcyd)_2]$ (**4**), and $[\{Mn(4\text{-}Clpcyd)(EtOH)(phen)\}_2(\mu\text{-}4\text{-}Clpcyd)_2]$ (**5**); hydrogen atoms are omitted for clarity. *Color code*: Mn (*pink*), C (*gray*), O (*red*), N (*blue*), F (*light blue*), Cl (*green*)

Results and discussion

*Mononuclear [Mn(3-Clpcyd)(H_2O)-(phen)$_2$]$^+$ (**1**)*

The geometry of the mononuclear complex **1** was optimized using MM and DFT methods. A new force field for these type of complexes was developed for this purpose (Table 1S). Energy minimization and geometry optimization resulted in one stable structure, which was in good agreement with the X-ray structure [31]. The structural parameters for the resulting energy-minimized structure obtained by MM and DFT calculations and comparison with the available crystallographic data for the complex ion **1** are presented in Table 1. As expected, the local density approximation (LDA) underestimates the bond lengths, while the Perdew-Burke-Erzerhoff (OPBE) exchange-correlation functional gives better results for the bond distances.

Calculations of the *g*-tensor and zero-field splitting parameters were carried out on the X-ray structure of [Mn(3-Clpcyd)(H_2O)-(phen)$_2$]$^+$ [31]. The calculated *g*-values for complex **1** are isotropic, with $g_{iso} = 2.0021$ $g_{iso} = (g_1 + g_2 + g_3)/3$. Calculations are in good agreement with typical experimental and theoretical predictions for a high-spin d^5 configuration of the manganese ion [32].

Since all d metal orbitals are semi-occupied, in the case of high-spin d^5 configuration, there is no circulation of electronic charge upon rotation. Semi-occupied molecular orbitals (SOMO) and (SOMO-1) are σ antibonding in character. The other orbitals, (SOMO-2), (SOMO-3), and (SOMO-4), are π antibonding. This is why the orbital contribution to the total *g*-values is small, so the shifts in *g*-values are small as well.

Calculated zero-field splitting parameters and *D* contributions to it are given in Table 2 using two different methods, as indicated in the "Introduction." The analysis of *D* contributions, SS and SOC, calculated with CP and PK methods, reveals that about 60% of *D* corresponds to SS interactions (Table 2). The same range of results was obtained for many six-coordinated complexes by other authors [33–35].

The main contribution to D_{SOC} arises from α–α and β–β excitations. In the case of the high-spin d^5 configuration, these excitations belong to the metal–ligand charge transfer (MLCT) and the ligand–metal charge transfer (LMCT), and have negative signs. For D_{SS}, the 1-center contribution is the most important one. The prediction of the sign of *D* is not straightforward because it becomes ambiguous when *E*/*D* approaches the rhombic limit (*E*/*D* $\approx$ 1/3) [5]. It has been shown for Mn(II) complexes that the calculations are unreliable once *E*/*D* becomes larger than 0.2 [33]. From the results in Table 2, it emerges that the CP method yields *E*/*D* values slightly larger than 0.2 and gives more reliable results than the PK approach.

Thus, using computational chemistry methods it is possible to give a detailed explanation of the magnetic properties of the complex **1**, and to analyze more complicated cases, such as the binuclear complexes **2**–**5**.

Table 1 Selected average bond lengths (Å) and angles (°) for the resulting energy-minimized structure by MM and DFT (LDA and OPBE) and comparison with the available crystallographic data for the [Mn(3-Clpcyd)(H_2O)-(phen)$_2$]$^+$ complex ion (**1**)

	M–N	M–N_{ph}	M–O	NMN_{ph}	N_{ph}MN_{ph}	NMO	N_{ph}MO
X-ray	2.119	2.307	2.149	97.86	82.60	92.20	93.90
MM	2.133	2.286	2.000	95.76	86.04	86.90	91.90
OPBE	2.020	2.305	2.630	99.80	88.26	73.80	90.67
LDA	1.979	2.184	2.375	99.96	88.12	73.50	92.86

Table 2 Calculated zero-field splitting parameters and *D* contributions from coupled-perturbed (CP) and Pederson–Khanna (PK) methods for complex **1**

	CP method	PK method
D (cm^{-1})	−0.155	−0.148
D_{SOC} (cm^{-1})	−0.063	−0.051
α–α	−0.064	−0.058
β–β	−0.074	−0.066
α–β	0.047	0.033
β–α	0.029	0.040
D_{SS} (cm^{-1})	−0.093	−0.097
1-center	−0.078	−0.083
2-center-Coulomb	0.001	0.002
2-center-exchange	0.000	0.000
2-center-hybrid	−0.018	−0.018
E (cm^{-1})	−0.034	−0.037
E/*D*	0.217	0.249

Binuclear complexes

DFT optimization is straightforward if the spins of the two metal ions are ferromagnetically aligned. If the two spins are antiferromagnetically aligned, complications arise [10]. The molecules studied in this work show weak AF coupling. Hence, to optimize the geometries of the studied molecules, we used the molecular mechanics method with essentially the same parameters as developed for the mononuclear complex (Table 1S).

Energy minimization and geometry optimization resulted in one stable conformation for each structure of the binuclear complexes **2**–**5**. Structural parameters for the energy-minimized species of the binuclear complexes are in agreement with the corresponding values obtained from the X-ray results (Table 3) [31].

M–N and M–O bond distances in the optimized structures of all the binuclear complexes were slightly longer

Table 3 Selected average bond lengths (Å) and angles (°) for the resulting MM energy-minimized structures of binuclear complexes and comparison with the available crystallographic data

	M–N	M–O	N–C	NMN	$N_{ph}MO$	CNM	$CN_{ph}M$	$CN_{ph}MN$
[{Mn(3-Fpcyd)(MeOH)(phen)}$_2$(μ-3-Fpcyd)$_2$] (**2**)								
X-ray	2.147	2.228	1.162	103.00	82.25	157.7	114.2	12.90
MM	2.137	2.225	1.156	102.70	85.00	157.6	113.1	4.00
[{Mn(3-Fpcyd)(EtOH)(phen)}$_2$(μ-3-Fpcyd)$_2$] (**3**)								
X-ray	2.143	2.250	1.172	100.60	84.35	140.80	113.30	39.00
MM	2.142	2.260	1.166	99.40	86.65	142.90	111.00	46.80
[{Mn(3-Clpcyd)(MeOH)(phen)}$_2$(μ-3-Clpcyd)$_2$] (**4**)								
X-ray	2.236	2.220	1.222	95.00	85.10	146.60	122.00	28.50
MM	2.232	2.219	1.223	93.90	86.35	152.40	119.40	36.20
[{Mn(4-Clpcyd)(EtOH)(phen)}$_2$(μ-4-Clpcyd)$_2$] (**5**)								
X-ray	2.129	2.238	1.172	101.40	83.90	148.40	110.50	26.30
MM	2.132	2.230	1.171	100.60	86.70	152.70	113.00	31.90

Table 4 Comparison of DFT-calculated (MM and X-ray geometries) and measured exchange coupling constants J

Complex	J (cm^{-1}) (calculated on X-ray)	J_{exp} (cm^{-1})	J (cm^{-1}) (calculated on MM optimized)
[{Mn(3-Fpcyd)(MeOH)(phen)}$_2$(μ-3-Fpcyd)$_2$] (**2**)	−4.61	−3.34	−3.24
[{Mn(3-Fpcyd)(EtOH)(phen)}$_2$(μ-3-Fpcyd)$_2$] (**3**)	−2.23	−0.41	−0.30
[{Mn(3-Clpcyd)(MeOH)(phen)}$_2$(μ-3-Clpcyd)$_2$] (**4**)	−3.52	−2.89	−1.30
[{Mn(4-Clpcyd)(EtOH)(phen)}$_2$(μ-4-Clpcyd)$_2$] (**5**)	−3.65	−2.60	−1.55

than those in the optimized structure of the mononuclear complex. NMN bond angles were larger in the mononuclear than the corresponding angles in binuclear complexes. It has been shown [31] that factors favoring AF coupling are mainly related to distortions in the Mn–$(NCN)_2$–Mn region: greater AF coupling is expected for systems in which the bridging region is not *chair*-distorted or in which the NCN-pcyd mean plane lies coplanar to the $(NCN)_2$ plane. The distortion in the central Mn–$(NCN)_2$–Mn region is induced by the deformation of C–N–M–N torsion angle (Fig. 1). Complex **2** shows the smallest central ring distortion in comparison with the other binuclear complexes, while in complex **3** the largest deviation of the central ring from planarity is observed (Table 3).

Calculations of magnetic couplings and g-tensors were carried out on the X-ray structures of all the binuclear complexes under study. To test the reliability of the present force field, calculation of magnetic couplings was also carried out on the energy-minimum conformations found by MM. All calculated magnetic coupling parameters are consistent with the experimentally obtained values (Table 4) [31].

Calculations revealed that interactions are weakly antiferromagnetic, due to the bridging ring structure [31]. The trend in the calculated J parameter correlates with ring distortion. The highly distorted compound **3** has the highest value for the J parameter (Fig. 2). The magnetic orbitals of the binuclear complexes, given in Fig. 3, give rise to an exchange pathway with reasonable overlap.

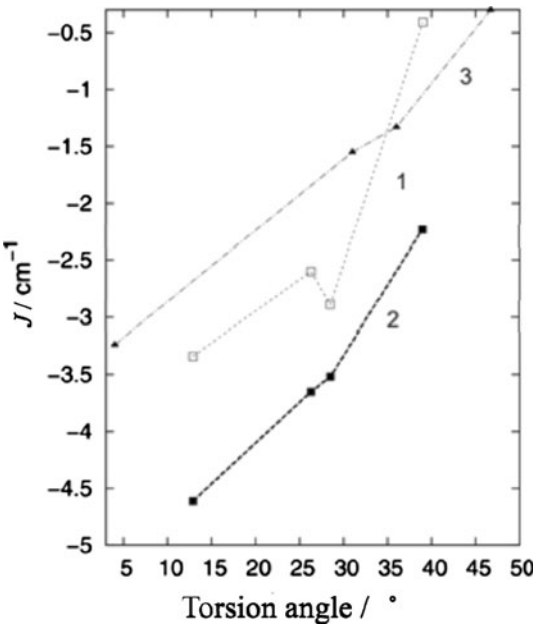

Fig. 2 Dependence of the J coupling parameters on the central ring distortion: *1* experimental values, *2* values calculated on X-ray structure, and *3* values calculated on MM-optimized structure

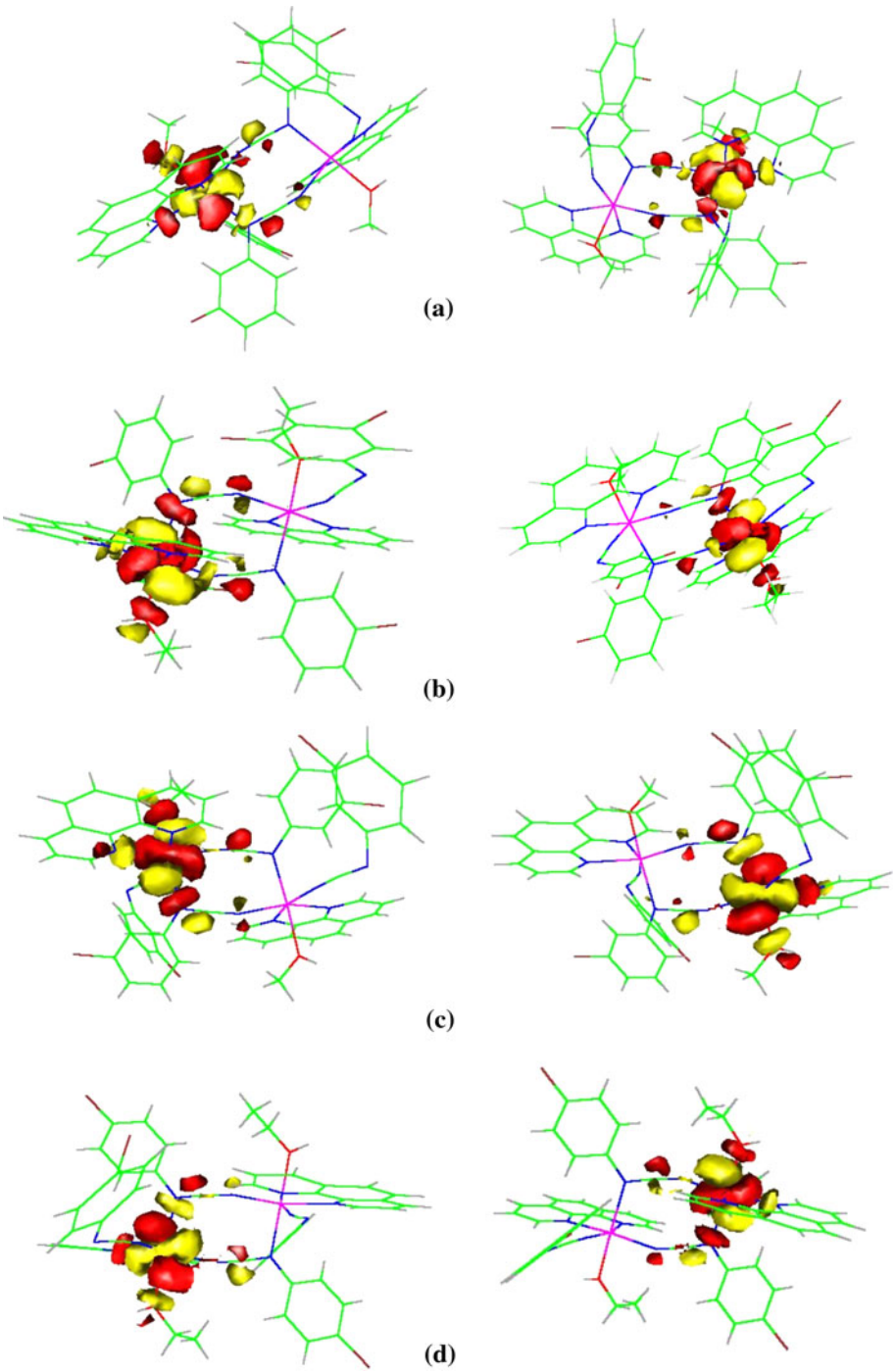

Fig. 3 Corresponding magnetic orbitals of **a** [{Mn(3-Fpcyd)(MeOH)(phen)}$_2$(μ-3-Fpcyd)$_2$] (**2**), **b** [{Mn(3-Fpcyd)(EtOH)(phen)}$_2$(μ-3-Fpcyd)$_2$] (**3**), **c** [{Mn(3-Clpcyd)(MeOH)(phen)}$_2$(μ-3-Clpcyd)$_2$] (**4**), and **d** [{Mn(4-Clpcyd)(EtOH)(phen)}$_2$(μ-4-Clpcyd)$_2$] (**5**)

It is evident that the antiferromagnetic couplings are present due to indirect exchange or superexchange, mediated via bridging ligand orbitals located between the two metal centers, so that the ligand forms a bond with both metal ions. The overlapping of ligand orbitals, which are located in the plane of the central ring, decreases with increasing distortion in the Mn–(NCN)$_2$–Mn region. Geometry changes between complexes **2** and **3** are due to the different molecule coordinated to the metal (EtOH, MeOH) and to the number of halogen atoms. These differences between the geometries of complexes **2** and **3** are responsible for the large differences in the values of *J*. MM is able to predict these geometry differences mainly localized in the Mn–(NCN)$_2$–Mn region.

As for the mononuclear complex, the calculated *g*-values for all analyzed binuclear complexes are isotropic, with the same value of $g_{iso} = 2.0019$.

Conclusions

We present a detailed study of the magnetic properties of mono- and homobinuclear Mn(II) complexes. We calculated the exchange coupling constants through the broken-symmetry DFT approach on X-ray and MM-optimized structures. Predominant antiferromagnetic interactions were always found, in line with experiment. The antiferromagnetic couplings are present due to indirect exchange or superexchange, mediated via bridging ligand orbitals located between the two metal centers. The calculated *g*-values for all investigated mono- and homobinuclear complexes are isotropic. Finally, the analysis of *D* contributions of mononuclear complexes, SS and SOC, reveals that about 60% of *D* corresponds to SS interactions. The same range of results is obtained for many six-coordinated complexes.

It is noteworthy that good agreement was obtained between MM calculated and experimental structures, not only in terms of metric data but also in the properties which depend on geometry, e.g., magnetic coupling parameters. This indicates that the present force field can be used with high accuracy to predict the geometries of similar complexes that have not yet been experimentally characterized, which could help in rational design of magnetic molecular materials.

Computational details

DFT calculations were performed using the Orca program package, version 2.5-15 [36]. Optimization of the mononuclear complex was performed using the LDA functional characterized by the Vosko–Wilk–Nusair (VWN) parametrization [37]. Beside the LDA functional, we also applied the OPBE functional [38, 39]. An all-electron Gaussian-type Ahlrichs triple-zeta valence basis set with three sets of first polarization functions (TZVPP) was used for the manganese atom, and a split valence basis set with one set of first polarization functions (SVP) for nonmetallic atoms [40, 41]. Calculations of magnetic couplings were done on X-ray and MM-optimized structures, using the B3LYP hybrid functional [42, 43, 45]. Electron paramagnetic resonance (EPR) *g*-values and ZFS parameters were calculated using the Becke '88 exchange and Perdew '86 correlation (BP86) functional [44, 45]. For EPR *g*-values the IGLO (III) basis set was used for all nonmetallic atoms [46].

Molecular mechanics (MM) calculations were carried out using the 2010/PC version of the Consistent Force Field (CFF) conformational program [47]. Conformational energy was defined in the usual way as given in Eq. 7:

$$E_{\text{total}} = \sum_r \frac{1}{2}k_r\left(r - r^0\right)^2 + \sum_\theta \frac{1}{2}k_\theta\left(\theta - \theta^0\right)^2 + \sum_\varphi \frac{1}{2}k_\varphi(1 + \cos n\varphi) + \sum_{ij}\left[\frac{2}{3}\varepsilon\left(\frac{r^*}{r}\right)^{12} - \varepsilon\left(\frac{r^*}{r}\right)^6\right] + \sum_{ij}\frac{e_i e_j}{Dr_{ij}}. \quad (7)$$

Bond-stretching and angle-bending contributions were treated with simple harmonic functions. Torsional contributions were represented as a Fourier series that accounts for all four torsions involving a double bond, or nine torsions involving a single bond. Nonbonded van der Waals interactions were computed with the Lennard–Jones "12-6" potential function. Nonbonded electrostatic contributions were modeled with the Coulomb function. Point charges were obtained from DFT calculations (ORCA).

The force field was parameterized on the basis of the three different types of carbon atom (sp hybridized C_{sp} atom of cyanamido ligand, aromatic carbon C_p, and sp^3 hybridized C_{sp3} atom), one type of oxygen atom, one type of hydrogen atom, two types of nitrogen atoms (sp^2 hybridized N atom and aromatic nitrogen N_{ph}), and the central metal atom Mn(II). Appropriate parameters were adjusted on a trial-and-error basis until we obtained the best agreement between calculated and X-ray structure for the mononuclear $[Mn(3\text{-Clpcyd})(H_2O)\text{-}(phen)_2]^+$ complex ion.

With essentially the same force field, we performed MM calculations on binuclear complexes. A list of all force-field parameters is given in Table 1S in the Supplementary Material. In the MM calculations, we treated the H_2O ligand as a single sphere with unique radius, compressibility, and charge [48].

Geometry optimizations were carried out using the combinations of the steepest-descent, Davidon–Fletcher–Powell, and Newton–Raphson methods [47]. Geometry optimizations were continued down to root-mean-square (rms) energy gradient of $<10^{-6}$ kJ/mol Å.

Acknowledgments This work was financially supported by the Serbian Ministry for Science through grant no. 172035.

References

1. Rajaraman G, Totti F, Bencini A, Caneschi A, Sessoli R, Gatteschi D (2009) Dalton Trans 45:3153
2. Bencini A, Casarin M, Forrer D, Franco L, Garau F, Masciocchi N, Pandolfo L, Pettinari C, Ruzzi M, Vittadini A (2009) Inorg Chem 48:4044
3. Bencini A, Totti F (2009) J Chem Theory Comput 5:44
4. Bencini A, Totti F (2005) Int J Quantum Chem 101:819
5. Duboc C, Ganyushin D, Sivalingam K, Collomb MN, Neese F (2010) J Phys Chem 114:10750
6. Pantazis DA, Kremwald V, Orio M, Neese F (2010) Dalton Trans 39:4959
7. Orio M, Pantazis DA, Petrenko T, Neese F (2009) Inorg Chem 48:7251
8. Ruiz E, Rodríguez-Fortea A, Cano J, Alvarez S, Alemany P (2003) J Comput Chem 24:982
9. Kahn O (1993) Molecular magnetism. VCH, New York
10. Neese F (2009) Coord Chem Rev 253:526
11. Pryce MHL (1950) Phys Rev 80:1107

12. Abragam A, Pryce MHL (1951) Proc Roy Soc 205:135
13. Noodleman L, Peng CY, Case DA, Mouesca JM (1995) Coord Chem Rev 144:199
14. Noodleman L, Case DA, Aizman A (1988) J Am Chem Soc 110:1001
15. Noodleman L, Norman JG, Osborne JH, Aizman A, Case DA (1985) J Am Chem Soc 107:3418
16. Noodleman L (1981) J Chem Phys 74:5737
17. Soda T, Kitagawa Y, Onishi T, Takano Y, Shigeta Y, Nagao H, Yoshika Y, Yamaguchi K (2000) Chem Phys Lett 319:223
18. Yamaguchi K, Takahara Y, Fueno T (1986) App Quantum Chem 155
19. Neese F (2003) Curr Opin Chem Biol 7:125
20. Neese F (2001) J Chem Phys 115:11080
21. Koseki S, Schmidt MW, Gordon MS (1998) J Phys Chem 102:10430
22. Koseki S, Schmidt MW, Gordon MS, Matsunaga N (1995) J Phys Chem 99:12764
23. Koseki S, Schmidt MW, Gordon MS (1992) J Phys Chem 96:10768
24. Bencini A, Gatteschi D (1990) EPR of exchange coupled systems. Springer, New York
25. Neese F (2004) In: Calculation of NMR and EPR parameters, theory and applications. Wiley-VCH, Weinheim
26. Neese F (2007) J Chem Phys 127:164112
27. Ray K, Begum A, Weyhermuller T, Piligkos S, van Slageren J, Neese F, Wieghardt K (2005) J Am Chem Soc 127:4403
28. Crutchley RJ (2001) Coord Chem Rev 125:219
29. Escuer A, Sanz N, Vicente R, Mautner FA (2003) Inorg Chem 42:541
30. Escuer A, Sanz N, Vicente R, Mautner FA (2003) Dalton Trans 11:2121
31. Escuer A, Mautner FA, Sanz N, Vicente R (2004) Polyhedron 23:1409
32. Duboc C, Collomb MN, Neese F (2010) Appl Magn Reson 37:229
33. Zein S, Duboc C, Lubitz W, Neese F (2008) Inorg Chem 47:134
34. Duboc C, Collomb MN, Pécaunt J, Deronzier A, Neese F (2008) Chem Eur J 14:6498
35. Pederson MR, Khanna SN (1999) Phys Rev 60:9566
36. Neese F (2006) Orca, an ab initio, DFT, and Semiempirical Electronic Structure Package, Version 2.8, Revision 15. Max-Planck-Institute für Bioanorganische Chemie, Mulhein
37. Vosko S, Wilk L, Nusair M (1980) Can J Phys 58:1200
38. Handy NC, Cohen AJ (2001) Mol Phys 99:403
39. Perdew JP, Burke K, Ernzerhof M (1996) Phys Rev Lett 77:3865
40. Schaefer A, Horn H, Ahlrichs R (1992) J Chem Phys 97:2571
41. Schaefer A, Huber C, Ahlrichs R (1994) J Chem Phys 100:5829
42. Becke AD (1986) J Chem Phys 84:4524
43. Perdew JP, Yue W (1986) Phys Rev 33:88001
44. Becke AD (1988) Phys Rev 38:3098
45. Perdew JP (1986) Phys Rev 33:8822
46. Kutzelnigg W, Fleischer U, Schindler M (1990) The IGLO-method: ab initio calculation and interpretation of NMR chemical shifts and magnetic susceptibilities. Springer, Heidelberg
47. Grubisic S, Gruden M, Niketic SR, Sakagami N, Kaizaki S (2002) J Mol Struct 609:1
48. Niketić SR, Rasmussen KJ (1977) The consistent force field: a documentation. Lecture notes in chemistry. Springer, Berlin, Germany